Advanced ultra-high-capacity optical random access memory and pattern recognition techniques

Hua-Kuang Liu, FELLOW SPIE
Yahong Jin, MEMBER SPIE
University of South Alabama
Department of Electrical and Computer Engineering
Mobile, Alabama 36688-0002
E-mail: hkliu@jaguar1.usouthal.edu

Neville I. Marzwell
California Institute of Technology
Jet Propulsion Laboratory
Pasadena, California 91109-8099

Abstract. The architecture and mathematical analysis of a new multichannel multistage holographic optical random access memory (HORAM) architecture and an experimental demonstration of its feasibility are presented. The new HORAM can be used for ultra-high-capacity storage and high-speed random retrieval of information. A two-stage HORAM, using a Dammann grating and a multifocus holographic lens, clearly shows the capability of storing 2000 holographic matched filters. The functional requirements for key optical elements including laser sources, spatial light modulators, and electro-optical shutters for making a desired practical and compact HORAM are described. The potential extension of the HORAM system for multiple-channel optical pattern recognition, classification, and image restoration are described. [S0091-3286(98)02503-3]

Subject terms: random access memory; optical pattern recognition; holographic lens; Dammann grating; optical pattern classification.

Paper ART-162 received July 2, 1997; revised manuscript received Aug. 19, 1997; accepted for publication Aug. 21, 1997.

1 Introduction

Instruments with high speed and large capacity *in situ* data identification, classification, and storage capabilities are required for information management and analysis. For example, in National Aeronautics and Space Administration (NASA) applications, extremely large volumes of data sets must processed in space exploration, space habitation and utilization, and in various missions to planet-earth programs. Parameters such as communication delays, limited resources, and inaccessibility of human manipulation require more intelligent, compact, low-power, and lightweight information management and data storage techniques.[1,2] For this reason, new and innovative techniques are being developed by many researchers in the field. Among the various techniques being developed, the 3-D volume holographic memory has been considered as one of the most important and promising for data storage.[3–11] For example, Mok[5] reported that more than thousands of holograms can be stored in a lithium niobate crystal via angular multiplexing, Heanue et al.[4] demonstrated the storage and retrieval of digital data using a volume hologram, and Yu and Yin have used a volume photorefractive crystal to make a reflection type matched filter applicable for pattern recognition.[11] The purpose of this paper is to present a new and basic concept of a multichannel multistage spatially parallel holographic optical random access memory (HORAM) system and the theoretical analysis of a two-stage HORAM architecture. The preliminary experimental results demonstrating the storage plane of a 2000-channel system and its potential for optical pattern recognition are presented. We then present various optical computing methods based on the HORAM architecture. The multistage HORAM can be used for the storage and random information retrieval among an extremely large amount of data and a family of pattern recognition applications. Advantages of the HORAM include large data storage capacity and high-speed parallel retrieval without moving parts. For a two-stage HORAM, two orders of magnitude of increment of the storage capacity can be achieved as compared with that of the single-staged spatial multiplexed multichannel optical pattern recognition system previously reported.[12–14] The practical limitations of the new architecture, primarily due to the availability of some basic components, are described at the end of the paper to stimulate further technology innovation and advancement required for this important technique.

2 Theoretical Discussion

The basic concept of the HORAM is shown in Fig. 1, where the input information T is presented in a 2-D image or data format, which is carried by a collimated laser beam. The input can either be presented with a phototransparency or in real time by a spatial light modulator. An example of an inexpensive laboratory type electronically addressed spatial light modulator is the liquid crystal television spatial light modulator[15] (LCTV SLM). The input T is then applied through a multiple number of cascaded stages of holographic optical elements (HOEs) and shutter arrays that are represented by the H blocks. Each H block may contain HOEs and shutter arrays. The functions of these elements are described by using blocks H_1 and H_2 as examples. The HOE in H_1 replicates input T into an array of $h_1 \times h_1$ identical T's. The shutter array in H_1 can be electronically controlled such that it can let any one of the $(h_1)^2$ replicas of T pass through and stop the others. The subsequent H_2 block

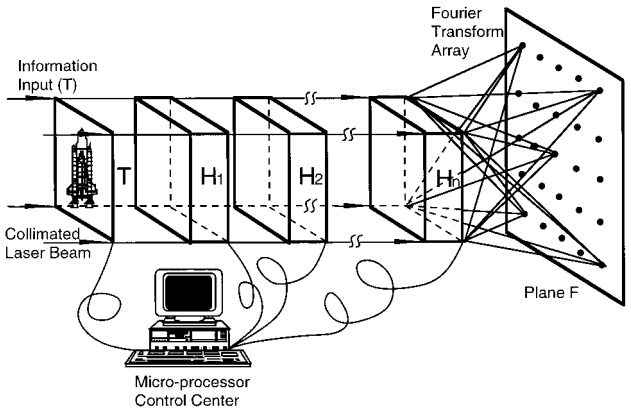

Fig. 1 Block diagram illustrating the concept of a HORAM.

has the function of a multifocus holographic lens with $(h_2)^2$ foci. A second shutter array can be used to select one of the foci of the multifocus lens. Hence at the output of the block H_2, $(h_1 \times h_2)^2$ Fourier transforms of T will appear one at a time at plane F since each time one of the Fourier transforms is selected, it is accomplished by the opening of one of each of the switches of the two shutter arrays. If one applies a reference beam to interfere with the Fourier transform, a holographic filter can be recorded at plane F. By using each Fourier transform in the array to record one of the images or 2-D data, a complete array of matched filters can be recorded. For example, if two H blocks are used with $h_1=9$ and $h_2=5$, a minimum of $(9\times5)^2=2025$ Fourier transforms of T can be stored at plane F if only one Fourier transform is recorded at each point of the array. Since holograms can be superpositioned, if each point is used to record four Fourier transforms by angular multiplexing, over 10,000 matched filters can be recorded at plane F. If $h_1=33$ and $h_2=7$ and a single matched filter at each focus is recorded, a total of 53,361 Fourier transforms of T can be stored at plane F. In the preceding examples, if the input data are images of human faces, then over 50,000 faces can be memorized in a HORAM. In the pattern recognition process, an input can be used to address all the stored holographic filters and therefore auto- or heterocorrelation signals can be obtained. On the other hand, by switching the shutter in each of the H blocks to let only one channel of the reference beam pass, one of the input images or 2-D data becomes randomly accessible.

One possible implementation of the HORAM in a two-stage architecture is to use a high-efficiency Dammann phase grating[16,17] with a lens and a shutter for H_1, and a multifocus holographic lens[18] (hololens) with a shutter for H_2. The transmission of the Dammann grating can be described as[19]

$$t(x,y)=\left[\text{comb}\left(\frac{x}{L_d},\frac{y}{L_d}\right)*g(x,y)\right]a(x,y), \tag{1}$$

where * indicates the convolution operator; L_d is the period of grating; $g(x,y)$ is the shape of the individual groove;

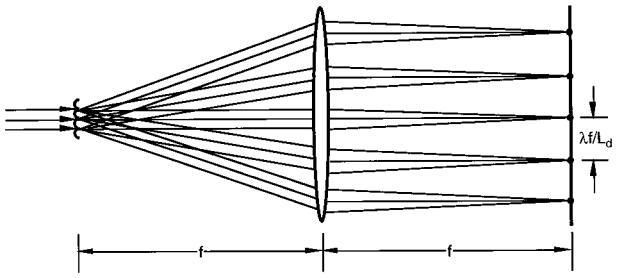

Fig. 2 Diffraction of light passing through a Dammann grating and a lens.

and $a(x,y)$ is the aperture, which in general is the incident Gaussian profile of the laser beam. However, for simplicity, the aperture is assumed to be open and uniform, so that $a(x,y)=1$. The Fourier transform of the grating[19] is

$$\begin{aligned}T(f_x,f_y)&=L_d^2[\text{comb}\ (L_df_x,L_df_y)]G(f_x,f_y)\\&=\sum_{m=-\infty}^{\infty}\sum_{n=-\infty}^{\infty}\delta\left(f_x-\frac{m}{L_d}\right)\delta\left(f_y-\frac{n}{L_d}\right)G(f_x,f_y),\end{aligned} \tag{2}$$

where $G(f_x,f_y)$ is the Fourier transform of $g(x,y)$, and $G(f_x,f_y)$ acts as a window function to attenuate those peaks of $\Sigma_{m=-\infty}^{\infty}\Sigma_{n=-\infty}^{\infty}\delta(f_x-m/L_d)\delta(f_y-n/L_d)$ that are not wanted. For a $(2M+1)\times(2M+1)$ array, we design the grating in such a manner that ideally

$$G(f_x,f_y)=\begin{cases}1 & |m|,|n|\leq M\\ 0 & |m|,|n|>M.\end{cases} \tag{3}$$

With Eq. (3), Eq. (2) can be expressed as

$$T(f_x,f_y)=\sum_{m=-M}^{M}\sum_{n=-M}^{M}\delta\left(f_x-\frac{m}{L_d}\right)\delta\left(f_y-\frac{n}{L_d}\right). \tag{4}$$

A traditional single-lens Dammann grating Fourier transform system is shown in Fig. 2.

A multifocus hololens[18] with its architecture and functionality as shown in Fig. 3 can be used as the HOE in H_2

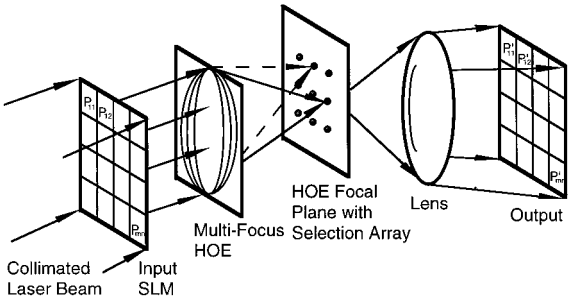

Fig. 3 Architecture and functionality of the multifocus hololens.

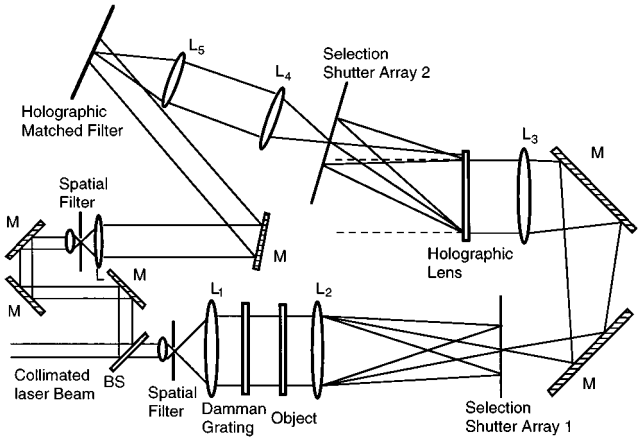

Fig. 4 Experimental setup of a HORAM system utilizing the cascade of a Dammann grating and a multifocus hololens.

of Fig. 1. The element was designed via a detailed Fourier computation and diffraction analysis[19] such that it will work as a lens with an array of foci. This multifocus hololens is different from an array of microlenses because the multifocus lens has a single aperture where the array of microlenses form foci, each of which has its own aperture. Therefore the multifocus hololens can be used to produce an array of Fourier transforms of the same input image where a microlens array cannot. For example, if the input to the multifocus hololens is a single laser beam, the beam can be directed to the array of foci with energy divided equally among the foci. When the input is an image carried by the collimated laser beam, in an ideal case, the multifocus hololens will produce at its focal plane an array of replicated Fourier transforms of the input. When one of the foci passes through a selection array spatial filter (in the form of small openings), it can be reimaged at the output plane. Special spectral modulation can be performed at the focal plane and image processing can be performed at the image plane. This architecture is therefore highly versatile. Moreover, by properly cascading the two HOEs as described, one can greatly increase the number of channels that can be processed in parallel. For example, the interconnection capacity and computation speed can hardly competed with by any other method.

The described HOEs can be invoked in an architecture, as shown in Fig. 4, as one way to implement the concept shown in Fig. 1. The architecture utilizes a cascaded combination of a Dammann phase grating and a multifocus hololens. A laser beam from an argon ion laser is divided into an object beam and a reference beam by a beamsplitter (BS). The object beam is collimated by a spatial filter and lens L_1 combination. The collimated beam is used to illuminate the Dammann grating and the input transparency so the output carries the input object. Lens L_2 is used to Fourier transform the object-carrying input beam multiplied by the transmittance of the Dammann grating into a $(2M+1)\times(2M+1)$ equal-intensity Fourier transform pattern array at the focal plane of L_2, where shutter array 1 is placed to selectively let one order pass in the recording process. The input pattern carried by the single diffraction order is imaged by L_3 to pass through the multifocus lens and is then Fourier transformed into the $(2N+1)\times(2N+1)$ foci array at the focal plane of the hololens, where N is the maximum diffraction order of the hololens. At the focal plane, the selection shutter array 2 is placed to selectively let one order to pass. Lenses L_4 and L_5 are used to reimage the passed Fourier transform where a holographic matched filter can be recorded. In the recording process, the reference beam is collimated by a spatial filter and lens L combination and is used to interfere with the Fourier transform of the object beam at the matched filter plane. If one let one object pass at each recording and let the reference beam to interfere only with that order, a total of $(2M+1)^2\times(2N+1)^2$ array of input data can be stored at the focal plane of L_5, as shown in Fig. 4. The data/image formation property of the HORAM shown in Fig. 4 is described in the following.

2.1 *Amplitude Distribution at Plane P_2 (Fourier Transform Plane of L_2)*

The object is illumined by an array of beams diffracted by the Dammann grating. The overall transmittance may be described as $t(x,y)O(x,y)$, where $t(x,y)$ and $O(x,y)$ are the transmittance functions of the Dammann grating and the object, respectively. Assuming that the combined grating-object is placed at one focal length in front of lens L_2, the result is an optically Fourier transformed array located at the back focal plane P_2 of L_2. The beam amplitude distribution at P_2 can be represented by a $(2M+1)\times(2M+1)$ array of Fourier transform of the object by lens L_2:

$$
\begin{aligned}
S_2(f_x,f_y) &= \frac{A}{j\lambda f_2}\,F_2[t(x,y)O(x,y)] \\
&= \frac{A}{j\lambda f_2}\sum_{m_d=-M}^{M}\sum_{n_d=-M}^{M}\delta\left(f_x-\frac{m_d}{L_d}\right) \\
&\quad\times\delta\left(f_y-\frac{n_d}{L_d}\right)*F_2[O(x,y)] \\
&= \frac{A}{j\lambda f_2}\sum_{m_d=-M}^{M}\sum_{n_d=-M}^{M}\delta\left(f_x-\frac{m_d}{L_d}\right) \\
&\quad\times\delta\left(f_y-\frac{n_d}{L_d}\right)*\tilde{O}(f_x,f_y),
\end{aligned}
\tag{5}
$$

where λ is the wavelength of the laser, A is a constant associated with the collimated laser input wave amplitude, f_2 is the focal length of lens L_2, $1/L_d$ is the period of the Dammann Grating in frequency domain, and F_n denotes the Fourier transform by lens $L_n(n=1,2,...)$,

$$\widetilde{O}(f_x,f_y)=F_2[O(x,y)]$$

$$=\int\int O(x,y)\exp\,[-j2\pi(f_x x+f_y y)]\,\mathrm{d}x\,\mathrm{d}y, \tag{6}$$

where f_x and f_y are the spatial frequencies: $f_x=x_2/(\lambda f_2)$ and $f_y=y_2/(\lambda f_2)$; and (x_2,y_2) are points in plane P_2. The amplitude distribution at P_2 can also be expressed in terms of the position at plane P_2:

$$U_2(x_2,y_2)=S_2\left(\frac{x_2}{\lambda f_2},\frac{y_2}{\lambda f_2}\right)$$

$$=\frac{A(\lambda f_2)^2}{j(\lambda f_2)}\sum_{m_d=-M}^{M}\sum_{n_d=-M}^{M}\delta\left(x_2-\frac{\lambda f_2}{L_d}m_d\right)$$
$$\times\delta\left(y_2-\frac{\lambda f_2}{L_d}n_d\right)*\widetilde{O}\left(\frac{x_2}{\lambda f_2},\frac{y_2}{\lambda f_2}\right)$$
$$=\frac{A}{j(\lambda f_2)}M_d(x_2,y_2)*\widetilde{O}\left(\frac{x_2}{\lambda f_2},\frac{y_2}{\lambda f_2}\right), \tag{7}$$

where

$$M_d(x_2,y_2)=(\lambda f_2)^2\sum_{m_d=-M}^{M}\sum_{n_d=-M}^{M}\delta\left(x_2-\frac{\lambda f_2}{L_d}m_d\right)$$
$$\times\delta\left(y_2-\frac{\lambda f_2}{L_d}n_d\right). \tag{8}$$

An aperture can be placed at plane P_2 with a selection filter, which is set to select one of the $(2M+1)\times(2M+1)$ equal-intensity diffraction orders.

2.2 *Amplitude Distribution at Fourier Plane of Lens L_3*

Lens L_3 is placed at distance f_3 from plane P_2. Due to the input at plane P_2, the amplitude distribution at the Fourier plane of lens L_3 can be written as

$$S_3(f_{x_2},f_{y_2})=\frac{1}{j\lambda f_3}F_3[U_2(x_2,y_2)]$$

$$=-\frac{A}{(\lambda f_2)(\lambda f_3)}F_3\{M_d(x_2,y_2)*F_2[O(x,y)]\}$$
$$=-\frac{A}{(\lambda f_2)(\lambda f_3)}F_3[M_d(x_2,y_2)]$$
$$\times F_3F_2[O(x,y)]. \tag{9}$$

The amplitude distribution Eq. (9) can also be expressed in terms of the position at Fourier plane of lens L_3, that is

$$U_3(x_3,y_3)=S_3\left(\frac{x_3}{\lambda f_3},\frac{y_3}{\lambda f_3}\right)$$

$$=-\frac{A(\lambda f_2)^2}{(\lambda f_2)(\lambda f_3)}\widetilde{M}_d\left(\frac{x_3}{\lambda f_3},\frac{y_3}{\lambda f_3}\right)$$
$$\times O\left(-\frac{f_2}{f_3}x_3,-\frac{f_2}{f_3}y_3\right), \tag{10}$$

where

$$\widetilde{M}_d(f_x,f_y)=F_3\{M_d(x,y)\}.$$

2.3 *Amplitude Distribution at the Fourier Plane of the Holographic Lens*

The holographic lens Fourier transforms the input $U_3(x_3,y_3)$ to a $(2N+1)\times(2N+1)$ array of spectrum onto its Fourier transform plane. The amplitude distribution is

$$S_h(f_{x_3},f_{y_3})$$

$$=\frac{1}{j\lambda f_h}\sum_{m_h=-N}^{N}\sum_{n_h=-N}^{N}\delta\left(f_{x_3}-\frac{m_h}{L_h}\right)\delta\left(f_{y_3}-\frac{n_h}{L_h}\right)$$
$$*F_h[U_3(x_3,y_3)]$$
$$=-\frac{A(\lambda f_2)^2}{j(\lambda f_2)(\lambda f_3)(\lambda f_h)}$$
$$\times\sum_{m_h=-N}^{N}\sum_{n_h=-N}^{N}\delta\left(f_{x_3}-\frac{m_h}{L_h}\right)\delta\left(f_{y_3}-\frac{n_h}{L_h}\right)$$
$$*F_h\left[\widetilde{M}_d\left(\frac{x_3}{\lambda f_3},\frac{y_3}{\lambda f_3}\right)\right]*F_h\left[O\left(-\frac{f_2}{f_3}x_3,-\frac{f_2}{f_3}y_3\right)\right]$$
$$=-\frac{A}{j(\lambda f_2)(\lambda f_3)(\lambda f_h)}$$
$$\times\sum_{m_h=-N}^{N}\sum_{n_h=-N}^{N}\delta\left(f_{x_3}-\frac{m_h}{L_h}\right)\delta\left(f_{y_3}-\frac{n_h}{L_h}\right)$$
$$*F_hF_3[M_d(x_2,y_2)]*F_hF_3\left[\widetilde{O}\left(\frac{x_2}{\lambda f_2},\frac{y_2}{\lambda f_2}\right)\right]. \tag{11}$$

The amplitude distribution [Eq. (11)] can also be expressed in terms of the position at the Fourier plane of the holographic lens, that is

$$
\begin{aligned}
&U_h(x_h,y_h)\\
&\quad=S_3\left(\frac{x_h}{\lambda f_h},\frac{y_h}{\lambda f_h}\right)\\
&\quad=-\frac{A(\lambda f_3)^4(\lambda f_h)^2}{j(\lambda f_2)(\lambda f_3)(\lambda f_h)}\\
&\qquad\times\sum_{m_h=-N}^{N}\sum_{n_h=-N}^{N}\delta\left(x_h-\frac{\lambda f_h}{L_h}m_h\right)\delta\left(y_h-\frac{\lambda f_h}{L_h}n_h\right)\\
&\qquad*M_d\left(-\frac{f_3}{f_h}x_h,-\frac{f_3}{f_h}y_h\right)*\widetilde{O}\left(-\frac{f_3}{\lambda f_2 f_h}x_h,\right.\\
&\qquad\left.-\frac{f_3}{\lambda f_2 f_h}y_h\right)\\
&\quad=-\frac{A(\lambda f_3)^4}{j(\lambda f_2)(\lambda f_3)(\lambda f_h)}M_h(x_h,y_h)\\
&\qquad*M_d\left(-\frac{f_3}{f_h}x_h,-\frac{f_3}{f_h}y_h\right)*\widetilde{O}\left(-\frac{f_3}{\lambda f_2 f_h}x_h,\right.\\
&\qquad\left.-\frac{f_3}{\lambda f_2 f_h}y_h\right),
\end{aligned}
\tag{12}
$$

where f_h is the focal length of the holographic lens, $1/L_h$ is the period of the holographic lens in the frequency domain, and

$$
\begin{aligned}
M_h(x_h,y_h)=(\lambda f_h)^2\sum_{m_h=-N}^{N}\sum_{n_h=-N}^{N}&\delta\left(x_h-\frac{\lambda f_h}{L_h}m_h\right)\\
&\times\delta\left(y_h-\frac{\lambda f_h}{L_h}n_h\right).
\end{aligned}
\tag{13}
$$

2.4 *Light Amplitude Distribution at the Matched Filter Plane*

For simplicity, L_4 and L_5 are selected as a pair of lenses with the same focal length f_4. Lens L_4 is placed at a distance f_4 from the Fourier plane of the holographic lens and lens L_5 is placed $2f_4$ from lens L_4. The matched filter plane is at the focal plane of lens L_5. The amplitude distribution at the matched filter plane can be expressed as

$$
\begin{aligned}
U_m(x_m,y_m)&=-\frac{1}{(\lambda f_4)^2}F_5F_4[U_h(x_h,y_h)]\\
&=-U_h\left(-\frac{f_4}{f_5}x_m,-\frac{f_4}{f_5}y_m\right).
\end{aligned}
\tag{14}
$$

Since $f_4=f_5$, we have

$$
\begin{aligned}
U_m(x_m,y_m)&=-U_h(-x_m,-y_m)\\
&=\frac{A(\lambda f_3)^4}{j(\lambda f_2)(\lambda f_3)(\lambda f_h)}M_h(-x_m,-y_m)\\
&\quad*M_d\left(\frac{f_3}{f_h}x_m,\frac{f_3}{f_h}y_m\right)\\
&\quad*\widetilde{O}\left(\frac{f_3}{\lambda f_2 f_h}x_m,\frac{f_3}{\lambda f_2 f_h}y_m\right),
\end{aligned}
\tag{15}
$$

where (x_m,y_m) is a point at the matched filter plane. It can be seen that the amplitude distribution at the matched filter plane is proportional to a $(N\times N)$ with $(M\times M)$ array of the Fourier transforms of the object

$$
\begin{aligned}
\widetilde{O}(f_x,f_y)&=F[O(x,y)]\\
&=\int\int O(x,y)\exp\left[-j2\pi(f_xx+f_yy)\right]\,dx\,dy,
\end{aligned}
$$

where

$$
f_x=\frac{f_3}{\lambda f_2 f_h}x_m\quad\text{and}\quad f_y=\frac{f_3}{\lambda f_2 f_h}y_m.
$$

2.5 *Recording of the Holographic Matched Filter*

In the recording of the holographic matched filter, two selection shutter arrays are placed at the plane P_2 and at the Fourier plane of the holographic lens, respectively. The shutter arrays are set such that only one order each from the Dammann grating and the holographic lens is selected to pass. Once the order (m_1,n_1) from Dammann grating and the order (m_2,n_2) from holographic lens are selected, the amplitude distribution at the matched filter plane, or Eq. (15), becomes

$$
\begin{aligned}
U_m(x_m,y_m)&=\frac{A(\lambda f_2)^2(\lambda f_3)^4(\lambda f_h)^2}{j(\lambda f_2)(\lambda f_3)(\lambda f_h)}\,\delta\left(-x_m-\frac{\lambda f_h}{L_h}m_2\right)\\
&\quad\times\delta\left(-y_m-\frac{\lambda f_h}{L_h}n_2\right)*\delta\left(\frac{f_3}{f_h}x_m-\frac{\lambda f_2}{L_d}m_1\right)\\
&\quad\times\delta\left(\frac{f_3}{f_h}y_m-\frac{\lambda f_2}{L_d}n_1\right)\\
&\quad*\widetilde{O}\left(\frac{f_3}{\lambda f_2 f_h}x_m,\frac{f_3}{\lambda f_2 f_h}y_m\right)\\
&=-jA(\lambda f_2)(\lambda f_3)(\lambda f_h)^3\delta\left(-x_m-\frac{\lambda f_h}{L_h}m_2\right)\\
&\quad\times\delta\left(-y_m-\frac{\lambda f_h}{L_h}n_2\right)*\delta\left(x_m-\frac{\lambda f_2 f_h}{f_3 L_d}m_1\right)\\
&\quad\times\delta\left(y_m-\frac{\lambda f_2 f_h}{f_3 L_d}n_1\right)\\
&\quad*\widetilde{O}\left(\frac{f_3}{\lambda f_2 f_h}x_m,\frac{f_3}{\lambda f_2 f_h}y_m\right),
\end{aligned}
\tag{16}
$$

or

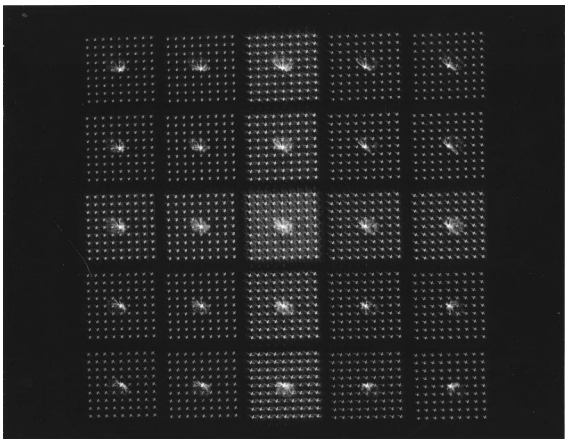

Fig. 5 Experimental demonstration: a 2025-channel (45×45) Fourier transform array at the plane *F* in Fig. 1 of a two-stage optical RAM.

$$U_m(x_m,y_m)=-jA(\lambda f_2)(\lambda f_3)(\lambda f_h)^3\tilde{O}\left(\frac{f_3}{\lambda f_2 f_h}x_m+\frac{f_3}{f_2 L_h}m_2-\frac{1}{L_d}m_1,\frac{f_3}{\lambda f_2 f_h}y_m+\frac{f_3}{f_2 L_h}n_2-\frac{1}{L_d}n_1\right), \quad (17)$$

where m_1 and n_1 range from $-M$ to M and m_2 and n_2 range from $-N$ to N. Once (m_1,n_1) and (m_2,n_2) are selected by shutter arrays 1 and 2, only one Fourier transform of the input image is recorded at matched filter plane. From this analysis, we can see that the total number of channels of the system is determined by the Dammann grating and the holographic lens used.

3 Experimental Demonstration

To show the feasibility of the HORAM, a preliminary experiment using the configuration shown in Fig. 4 was performed. In the experiment, we used a Dammann grating with $M=4$ $(2M+1=9)$ and a 25-foci hololens with $N=2(2N+1=5)$. A 25-mW Spectra Physics Model 164 He-Ne laser was used as the input laser source. Focal length of the lenses used in the system are $f_1=10$ cm, $f_2=20$ cm, and $f_3=f_4=f_5=38$ cm with corresponding apertures of 4 and 5 cm for L_1 and L_2 respectively, and 7.62 cm for the SORL lenses L_3, L_4, and L_5, the focal length of the hololens $f_h=25.4$ cm. The effective aperture used for the input image is about 5 mm. The experimental output of a two-stage HORAM at the mulplexed Fourier transform array output plane of Fig. 4 is shown in Fig. 5. A total of 2025 Fourier transforms in a 2-*D* array of 45×45 foci format has been obtained in an area of 2×2 cm at the matched filter plane. Matched filters at a single focus and several randomly selected focuses have been recorded and the correlation signals have been observed.

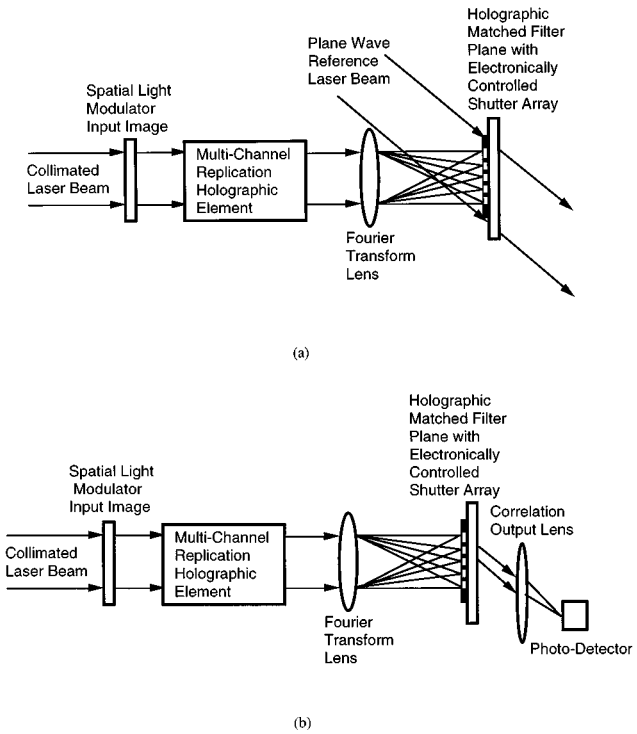

Fig. 6 (a) Multichannel pattern recognition system reording architecture and (b) multichannel pattern recognition system addressing architecture.

4 Optical Pattern Recognition and Computing Methods Based on the HORAM

The HORAM has a broad range of applications. Based on the multistage HORAM architecture, a few optical pattern recognition and special-purpose optical computing methods can be implemented as described next.

4.1 *Multichannel Pattern Recognition System*

The recording and addressing architecture of a multichannel pattern recognition system are shown, respectively, in Figs. 6(a) and 6(b). In Fig. 6(a), the object is presented to the system via a spatial light modulator illuminated by a collimated laser beam. The image is replicated in a similar manner as that in the HORAM as described. The replicated images form an array of Fourier transform patterns at the holographic matched filter plan where the matched filters can be made by using a single plane reference wave during the image storage process. For each image, a shutter is open to select one of the Fourier transform of the array. In the addressing process, if an input object image is one of the images stored, the output correlation signal will immediately reveal the answer. To give a numerical example, if the same image is rotated five times and stored in the same location of a matched filter, an array of 2000 would enable 10,000 images to be stored. The capacity of storage would allow recognition of images with rotation and scale variations.

4.2 *Multichannel Pattern Classification System*

The recording and addressing architecture of a multichannel pattern classification system are shown, respectively, in

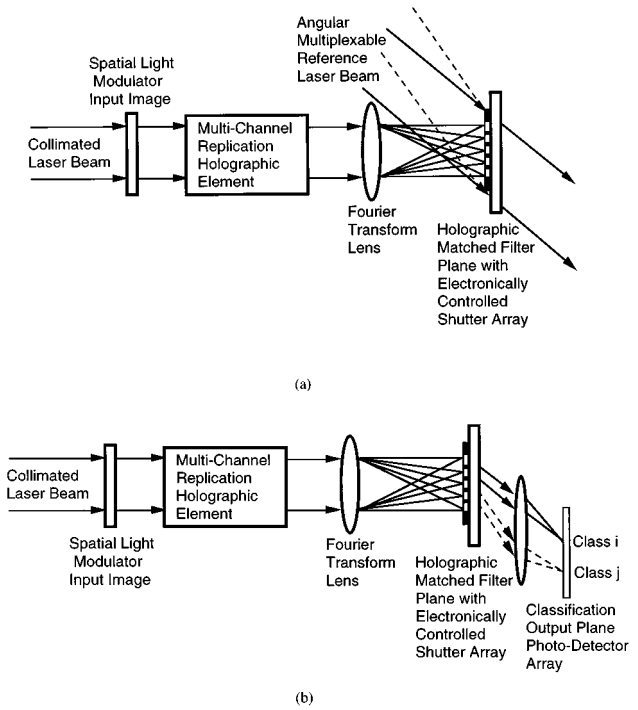

Fig. 7 (a) Multichannel pattern classification system recording architecture and (b) multichannel pattern classification system reording architecture.

Figs. 7(a) and 7(b). The recording and addressing processes are similar to those described in Sec. 4.1. The major difference is that in this case, an orientation variable plane wave is used for the image storage process. The images or features belong to the same class is stored with a certain selected orientation of the reference beam. In the addressing process, if an input object image is one of the class of the images stored, the position of the output correlation signal will immediately reveal the class that the image belongs to. For example, the 10,000 images of the example given in Sec. 4.1 can be classified into 100 classes by using 100 reference waves each of which is oriented at a distinctive angle.

4.3 *Multichannel Pattern Restoration System*

The recording and addressing architecture of a multichannel pattern restoration system are shown in Fig. 8. A single plane wave is used for all the image storage process similar

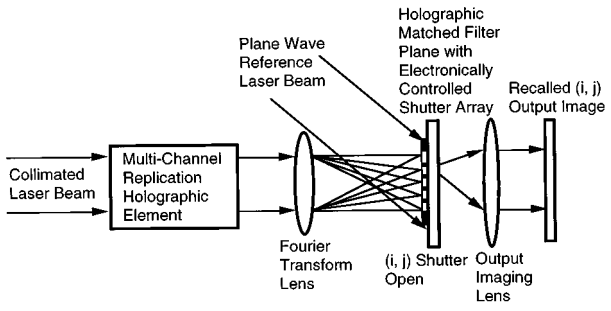

Fig. 8 Multichannel pattern restoration system addressing architecture.

Table 1 Desired SLM functional requirements.

Functional Features	Desired Specifications
Space-bandwidth product	1042×1042
Aperture dimensions (mm×mm)	5×5
Speed (frames/s)	1000
Dynamic range	100:1
Light efficiency	90%
Cost	$100 or less

to that of Fig. 6(a). In the image restoration process, the object beam is shut off and the (i,j)'th stored object image can be restored by using the same reference beam and electronically controlled selection shutters placed in front of the output imaging lens. The image stored at the (i,j)'th matched filter position will be holographically retrieved by the recording reference beam. In this case, only one image at each filter can be stored and recalled. The inverse Fourier transform is performed by the lens placed after the matched filter array. The restored image can be displaced at its focal plane.

5 Discussion

The definition and functional requirements for a traditional RAM have been realized electronically with impressive accomplishments and on-going progress in capacity, speed, and compactness. The optical RAM described in this paper is not intended to compete with the digital electronic RAM. The optical RAM architecture can offer an unique feature in high-speed parallel optical pattern recognition over an extremely large database. However, to achieve the special-purpose computing goals, technological advancement and breakthroughs in some of the key optical components are required. The challenges and opportunities in the research and development of the components are now briefly discussed.

5.1 *Laser Sources*

It is desired to have a laser source comparable to a laser diode in size with a power level comparable to that of an argon ion laser. However, the laser diodes have very poor coherent length and are not suitable for making holograms. The diode-pumped solid state laser has high power output but also lacks of coherence. Hence at the present time it is necessary to use large-frame lasers as recording sources.

5.2 *SLMs for Data Input*

The SLM for the input in the optical RAM poses a challenge for device technology development. Many kinds of SLMs have been developed. These include the Hughes liquid crystal light valve, the microchannel plate SLM, the microdeflection mirror SLM, the ferroelectric liquid crystal SLM, and the liquid crystal television SLM. For high-speed optical RAM operation, high-frame-rate SLMs with high dynamic range, small size, and large numbers of pixels are required. The desired functional requirements for the SLM are listed in Table 1.

No single currently available SLM has all the desired features, and the price of high-quality SLMs is too high to

use to construct a practical optical RAM. The liquid crystal television SLM is the only inexpensive SLM that meets the low-cost requirement, but it has other limitations including speed, contrast, and resolution.

5.3 *Optical Lenses and Mirrors*

To achieve optimum light utilization efficiency, Fourier optical lenses and mirrors must be specifically designed and fabricated. Ideally, a miniaturized optical system with an input lens of an effective aperture of less than 5×5 mm and with other components designed based on this aperture is desired.

5.4 *Shutter Arrays*

A single-aperture mechanical shutter can be used to write the input data into the memory. Mechanical shutters have an aperture of 100% transmittance. The position of the shutter can be precisely translated under the control of a PC. An alternative method is to use a liquid crystal shutter array. These shutters are available mostly in reflection mode with high distinction ratios. In the addressing mode, the shutters can be completely removed and hence will not affect the performance of the memory retrieval or pattern recognition functions.

5.5 *Holographic Recording Materials*

Candidates for real-time holographic recording materials include nonlinear photorefractive crystals, photopolymers, and thermoplastic materials. The recording sensitivity of the thermoplastic material is comparable to that of silver halide film. A simple and compact charging system must be developed for the thermoplastic recording device. More sensitive photorefractive and photopolymer materials must be developed for large-capacity memory.

5.6 *Output Detectors*

Photodiodes can be used for the detection of a single output signal. An array of output signals can be detected by a CCD array. Large-array position determinable smart pixel devices are required for pattern classification applications.

5.7 *Light Budget Estimate, Speed, and Applications*

Next, we make an estimate of the light budget for a two-stage HORAM based on realizable optical components. Assume a laser power of 5 W is used. The collimating optics reduces its power by a factor of 70%, the input SLM reduces its power by a factor of 90%, the Dammann grating by 80%, the hololens by 50%, and each of the shutter arrays by 50%. Since part of the beam is used by the reference beam, another factor of 90% will be multiplied, miscellaneous light loss of the components is represented by a factor of 70%. The overall factor is the multiplication of all the factors. The resulting factor is about 4%. By dividing the resulting light power by 2000, a maximum of 100 μW is available for the recording of a single matched filter. The same power level is available for retrieval. If the matched filter has a 50% diffraction efficiency, the correlation signal has an output of at most 50 μW, which is sufficient for the detection devices. Based on this estimate, the power levels will reach its limit if we have a 10,000-channel HORAM.

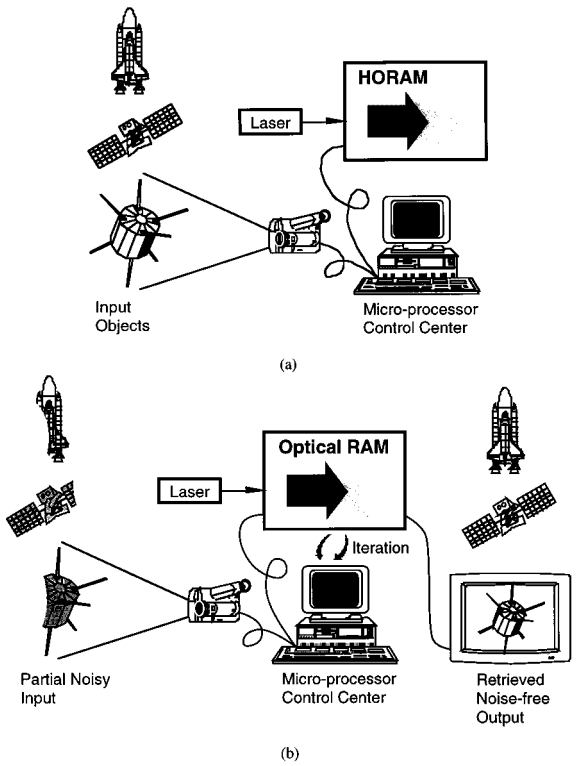

Fig. 9 Examples of HORAM applications: (a) memory process and (b) information retrieval.

The retrieval and processing speed is limited by that of the input SLM. For a 10,000-channel HORAM, if all the optimum values of the parameters are used and we assume that the speed the input SLM is 1000 frames/s with 400 $\times$600 binary pixels, the processing speed is estimated to be 240 Gbits/s. This speed for pattern recognition is valuable for certain specific applications.

With respect to the applications of these specific optical computing methods, one example of these applications is illustrated in Fig. 9. Figure 9(a) shows how memorization is accomplished in the HORAM by placing the objects as represented by the satellite and space shuttle in the view of a video camera. Over tens of thousands of 2-D data can be stored. Microprocessors can be used to control the random access to any data set from the memory. After the HORAM memorizes all the images presented to it, it becomes smart. When an input such as a partial and noisy space shuttle, as shown in Fig. 9(b), is presented to it, the HORAM can recover and display at the output screen the perfectly retrieved image. In addition, the HORAM can be used to recognize an input and tells us whether it belongs to the memory. For example, if the fingerprints of FBI's most wanted criminals are stored in the memory, the HORAM can determine whether an arbitrary input fingerprint belongs to one of the criminals. The recognition can be accomplished remotely and the HORAM can make a decision at the speed of light!

6 Conclusions

We have described a new technique of using multiple stages of free-space interconnection holographic elements

to implement a HORAM. We have demonstrated the technique with a memory capacity of over 2000 images. Potentially, seemingly limited only by the laser power, tens of thousands of images can be stored. Microprocessors can be used to control the random access to any data set from the memory. Each of the thousands of Fourier transforms in the array can be used to record a matched filter of an input image. Simultaneous optical pattern recognition and/or data processing of the superlarge array means a computing speed of the order of at least 10^{11} bits/s. This speed is faster than those obtainable by any other methods reported. For example, if the fingerprints of FBI's most wanted criminals are stored in the memory, the HORAM can determine whether an arbitrary input fingerprint belongs to one of the criminals. The recognition can be accomplished remotely and the HORAM can make the decision at the speed of light!

Acknowledgments

The research work was performed jointly at the Jet Propulsion Laboratory, California Institute of Technology, and the University of South Alabama. The work was supported by (1) NASA Advanced Concepts Research Fellowship Grant No. NAG 2-1050; (2) NASA Contract No. NAS7-1307 with the Standard International Corporation, Lumin, Inc., the University of South Alabama, and the University of California at Santa Barbara; (3) Department of Energy (DOE) contract DE-AC05-84OR2140 to the Oak Ridge National Laboratory (ORNL) and ORNL's Subcontract No. 85X-ST933V to Lumin, Inc.; and (4) DOE Alabama EPSCoR Young Investigator subcontract to University of South Alabama. Helpful technical discussions with Fred Aminzadeh and Jacob Barhen are hereby acknowledged.

References

1. B. J. Goertzen and P. A. Mitkas, ''Volume holographic storage for large relational databases,'' *Opt. Eng.* **35**(7), 1847–1853 (1996).
2. P. B. Berra, A. Ghafoor, P. A. Mitkas, S. J. Marcinkowski, and M. Guizani, ''The impact of optics on data and knowledge base systems,'' *IEEE Trans. Knowl. Data Eng.* **11**, 111–132 (1989).
3. N. V. Kukhtarev, V. B. Markov, S. G. Odulov, M. S. Soskin, and V. L. Vinetskii, ''Holographic storage in electrooptic crystals, I. Steady state,'' *Ferroelectrics* **22**, 949–964 (1979).
4. J. F. Heanue, M. C. Bashaw, and L. Hesselink, ''Volume holographic storage and retrieval of digital data,'' *Science* **265**(5173), 749–752 (1994).
5. F. H. Mok, ''Angle-multiplexed storage of 5000 holograms in lithium niobate,'' *Opt. Lett.* **18**, 915–917 (1993).
6. S. Yin, H. Zhou, F. Zhao, M. Wen, Z. Yang, and F. T. S. Yu, ''Wavelength multiplexed holographic storage in a sensitive photorefractive crystal using a visible light tunable diode laser,'' *Opt. Commun.* **101**, 317–321 (1993).
7. P. A. Mitkas and L. J. Irakliotis, ''Three-dimensional optical storage for database processing,'' *J. Opt. Mem. Neural Net.* **3**(2), 87–98 (1994).
8. J. H. Hong, I. McMichael, T. Y. Chang, W. Christian, and E. G. Paek, ''Volume holographic memory systems: techniques and architectures,'' *Opt. Eng.* **34**(8), 2193–2203 (1995).
9. D. Psaltis, ''Parallel optical memories,'' *Byte* **17**(9), 179–182 (1992).
10. J. R. Wullert II and Y. Lu, ''Limits of capacity and density of holographic storage,'' *Appl. Opt.* **33**(11), 3192–3196 (1994).
11. F. T. S. Yu and S. Yin, ''Thick volume photorefractive crystal wavelength-multiplexed reflection-type matched filter,'' *Opt. Mem. Neural Net.* **3**, 207–214 (1994).
12. D. Gregory, G. Duthie, and H. K. Liu, ''Large memory real-time multichannel multiplexed pattern recognition,'' *Appl. Opt.* **23**, 4560–4570 (1984).
13. H. K. Liu, J. Barhen, and N. Farhat, ''Unipolar terminal-attractor based neural associative memory with adaptive threshold,'' U.S. Patent No 5,544,280 (Aug. 1996).
14. H. K. Liu and J. Wu, ''Optical implementations of terminal-attractor based associative memory,'' *Appl. Opt.* **31** 4631–4644 (1992).
15. H. K. Liu and T. H. Chao, ''Liquid crystal television spatial light modulators,'' *Appl. Opt.* **28**, 4772–4780 (1989).
16. H. Dammann and K. Grotler, ''High-efficiency in-line multiple imaging by means of multiple phase holograms,'' *Opt. Commun.* **3**, 312–315 (1971).
17. M. Blume, F. B. McCormick, P. J. Marchand, and S. C. Esener, ''Array interconnect systems based on lenslets and CGH,'' *Proc. SPIE* **2537**, 180–193 (1995).
18. Y. Z. Liang, D. Z. Zhao, and H. K. Liu, ''Multifocus dichromated gelatin hololens,'' *Appl. Opt.* **22**, 3451–3459 (1983).
19. J. W. Goodman, *Introduction to Fourier Optics*, McGraw-Hill, New York (1968).

Hua-Kuang Liu is a professor of electrical engineering at the University of South Alabama (USA) and a Distinguished Visiting Scientist at the Center for Engineering Systems Advanced Research of the Oak Ridge National Laboratory. Before joining USA in September 1995, Dr. Liu was a senior research scientist with the Jet Propulsion Laboratory (JPL), California Institute of Technology. He received his PhD degree in electrical engineering from Johns Hopkins University. Dr. Liu was a professor of electrical engineering at the University of Alabama from 1969 to 1984, has presented many invited talks, seminars, and short courses at national and international meetings and universities, and was a record holder as the three-time recipient of the Best Faculty Research Award awarded by the Capstone Engineering Society in the years 1979, 1982, and 1984. In research, Dr. Liu has managed and directed major R&D projects sponsored by National Aeronautics and Space Administration (NASA), Department of Defense, and Department of Energy agencies and industries. He has been a group leader of advanced optoelectronic computing and information processing R&D groups at JPL. Dr. Liu's research specialties include optoelectronic computing, high-volume data storage and random access memory, information processing, and neural networks. During the last decade, Dr. Liu has acquired and managed contracts and projects totaling over $7 million. In new technology development, he holds over 27 U.S. patents and NASA Awards and Certificates of Recognition for Technology Innovation. He was recognized by the Caltech Patent Office as the most prominent inventor in modern optics in the history of NASA/JPL. Dr. Liu has published more than 200 technical papers, has participated in many university committees, has organized and chaired over 30 national and international conferences, and has served as a referee for archival journals and as a reviewer for major funding agencies. In 1975, Dr. Liu founded a high-tech firm, Lumin Inc., which has made many important cutting edge technology discoveries. Dr. Liu is a fellow of the OSA and SPIE and is listed in several national and international Who's Who publications.

Yahong Jin received her PhD degree in physics from the Rensselaer Polytechnic Institute, Troy, New York, and her BS and MS degrees from Shanghai Jiao Tong University, Shanghai, China. Since 1995, she has been a visiting assistant professor of electrical engineering at the University of South Alabama, Mobile. From 1994 to 1995, she was a visiting scientist at the Advanced Optoelectronic Computing Laboratory of the Jet Propulsion Laboratory, California Institute of Technology, Pasadena, working on optical information processing, pattern recognition, and holography. Her current research interests include optoelectronic computing and holography, ultrafast electromagnetic switching and optical communications, nonlinear crystals, and optical memory and data storage. Dr. Jin has published over 20 refereed journal papers and one book chapter and has made over 20 presentations at national and international conferences. She is a member of the IEEE, the American Physical Society, and SPIE.

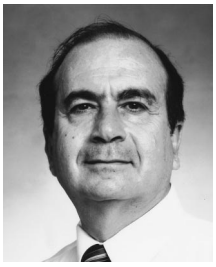

Neville I. Marzwell is project manager for advanced concepts and technology innovation at the Jet Propulsion Laboratory (JPL), California Institute of Technology, Pasadena, and has 25 years experience in defense and aerospace systems technologies in which he initiated various technology innovations. His area of expertise is large optical systems for imaging far fainted objects and high energy lasers. He has developed adaptive, distributive, and hierarchical control systems for large space structures and has contributed developments in autonomous space systems, robotics, and teleoperated systems. Before joining JPL, he was program manager of advanced technology with the High Energy Laser Research at the Rockedyne Division of Rockwell International, where he developed innovative wavefront sensing and correction systems and optical and sensor protection systems for surveillance satellites. At Honeywell Research Center he was instrumental in advances in IR detector technology, electro-optical materials, and fiber optical systems. Dr. Marzwell was a Josephine de Karman fellow at the California Institute of Technology and holds a PhD in applied physics and materials science from Caltech. He has published 55 papers in refereed and professional journal and has served on various national and international panels and workshop, conferences, and symposium committees.